

Article

Open Access



Protective behavior of phosphonate-functionalized imidazolium ionic liquid and its impact on the Li-ion battery performance

Kaisi Liao^{1,#}, Jingbo Song^{1,#}, Jiawen Ge^{1,#}, Jia Si¹, Yinxiao Cai¹, Zijuan Luo¹, Mingjiong Zhou^{1,*}, Hongze Liang^{1,*}, Ya-Jun Cheng^{2,†}, Marija Milanovic³, Atsushi Inoishi⁴, Shigeto Okada⁴

¹School of Materials Science and Chemical Engineering, Ningbo University, Ningbo 315211, Zhejiang, China.

²Ningbo Institute of Materials Technology & Engineering, Chinese Academy of Sciences, Ningbo 315201, Zhejiang, China.

³Department of Materials Engineering, Faculty of Technology Novi Sad, University of Novi Sad, Novi Sad 21000, Serbia.

⁴Institute for Materials Chemistry and Engineering, Kyushu University, Kasuga 816-8580, Japan.

[#]The authors contributed equally.

* **Correspondence to:** Prof./Dr. Mingjiong Zhou, School of Materials Science and Chemical Engineering, Ningbo University, 818 Fenghua Road, Jiangbei District, Ningbo 315211, Zhejiang, China. E-mail: zhoutingjiong@nbu.edu.cn; Prof./Dr. Hongze Liang, School of Materials Science and Chemical Engineering, Ningbo University, 818 Fenghua Road, Jiangbei District, Ningbo 315211, Zhejiang, China. E-mail: lianghongze@nbu.edu.cn; Prof./Dr. Ya-Jun Cheng, Ningbo Institute of Materials Technology & Engineering, Chinese Academy of Sciences, 1219 Zhongguan West Road, Ningbo 315201, Zhejiang, China. E-mail: chengyj@nimte.ac.cn

How to cite this article: Liao K, Song J, Ge J, Si J, Cai Y, Luo Z, Zhou M, Liang H, Cheng YJ, Milanovic M, Inoishi A, Okada S. Protective behavior of phosphonate-functionalized imidazolium ionic liquid and its impact on the Li-ion battery performance. *Energy Mater* 2023;3:300044. <https://dx.doi.org/10.20517/energymater.2023.33>

Received: 28 Apr 2023 **First Decision:** 2 Jun 2023 **Revised:** 23 Jun 2023 **Accepted:** 13 Jul 2023 **Published:** 10 Oct 2023

Academic Editors: Yuping Wu, Giovanni Battista Appetecchi **Copy Editor:** Fangyuan Liu **Production Editor:** Fangyuan Liu

Abstract

The commercial lithium-ion batteries (LIBs) rely on lithium hexafluorophosphate (LiPF₆), which is extremely sensitive to moisture and liable to thermal decomposition. Lithium bis (trifluoro methane sulfonyl) imide (LiTFSI), as a promising electrolyte salt, possesses high thermal stability and excellent moisture tolerance. However, LiTFSI is closely related to severe corrosion of the aluminum (Al) current collector at high voltage. Herein, phosphonate-functionalized imidazolium ionic liquid (PFIL) is developed and utilized as an electrolyte co-solvent to inhibit the oxidative dissolution of the Al current collector. PFIL can suppress Al corrosion by participating in the interface reaction and forming a stable and reliable protective film on the surface of Al foils, as confirmed by X-ray photoelectron spectroscopy. Thanks to the corrosion suppression of the Al current collector, the Li||LiNi_{0.8}Mn_{0.1}Co_{0.1}O₂ (NCM811) cells with PFIL-containing electrolytes exhibit better cycling performance and improved capacity retention. This work proposes an effective strategy for the advancement of high-voltage LIBs and contributes to promoting the widespread use of the sulfone imide-based lithium salts.



© The Author(s) 2023. **Open Access** This article is licensed under a Creative Commons Attribution 4.0 International License (<https://creativecommons.org/licenses/by/4.0/>), which permits unrestricted use, sharing, adaptation, distribution and reproduction in any medium or format, for any purpose, even commercially, as long as you give appropriate credit to the original author(s) and the source, provide a link to the Creative Commons license, and indicate if changes were made.



Keywords: Electrolyte, aluminum corrosion, ionic liquid, lithium-ion battery, lithium bis (trifluoro methane sulfonyl) imide

INTRODUCTION

Lithium hexafluorophosphate (LiPF_6) is the most widely used lithium salt for commercial lithium-ion batteries (LIBs)^[1]. However, the LiPF_6 salt is extremely sensitive to moisture and susceptible to thermal decomposition ($125\text{ }^\circ\text{C}$)^[2-5]. The decomposition product of phosphorus pentafluoride (PF_5) of LiPF_6 is a strong Lewis acid^[6,7], which initiates the decomposition of cyclic carbonate. When PF_5 reacts with a trace amount of water, active hydrogen fluoride (HF) will corrode a solid electrolyte interphase (SEI) layer, dissolve the cathode, and deteriorate the electrochemical performance of the LIBs^[8-11].

To overcome these problems, researchers are devoted to seeking a stable lithium salt to replace LiPF_6 ^[12-15]. Because of excellent thermal and moisture stability ($360\text{ }^\circ\text{C}$), high ionic conductivity, and good electrochemical stability, lithium bis (trifluoro methane sulfonyl) imide (LiTFSI) is considered as a promising electrolyte salt for use in the LIBs^[12,16,17]. The operation temperature range and safety performance of the LIBs are enhanced by using LiTFSI instead of LiPF_6 . For these reasons, intensive studies have been conducted on the LiTFSI-based electrolyte^[18-21]. However, the application of LiTFSI is constrained by severe corrosion of the Al current collector ($\sim 3.7\text{ V vs. Li/Li}^+$)^[22-24]. The urgent resolution of the corrosion issue of the Al current collector becomes more imperative when it is matched with high-voltage cathode materials.

The LiTFSI-based electrolyte causes continuous dissolution of alumina and aluminum (Al) because it fails to form an effective passivation layer on the Al current collector^[25]. The corrosion of the Al current collector can be partially alleviated by adjusting the proportion of lithium salts and utilization of functional additives to form a protective layer over the Al current collector. Matsumoto *et al.* proposed that high concentration LiTFSI (1.8 M) electrolyte formed a LiF passivation layer on Al current collector, which could inhibit the corrosion^[26]. Li *et al.* proved the formation of a boron-based passivation layer by oxidative decomposition of lithium difluoro(oxalate)borate (LiODFB) to suppress the dissolution of Al current collectors^[23]. Although these additives can mitigate the corrosion of Al current collectors, their practical application is limited due to their incompatibility with positive electrode materials, resulting in poor electrochemical stability at high potentials.

Ionic liquids (ILs) show various unique properties, such as non-flammability, non-volatility, and wide high-voltage stability window, which are considered as ideal high-potential electrolyte additives to replace part of the organic carbonates^[27,28]. Peng *et al.* suggested that the Al current collector was stable in the IL electrolyte, which was attributed to a good passivation layer formed by the oxidation between Al and the anions of the IL electrolyte^[29]. Therefore, ILs are expected to have the ability to suppress the Al current collector corrosion.

Among various types of ILs, imidazolium-based ILs are the most studied due to their low viscosity and high conductivity^[30]. Nevertheless, the acidic hydrogen at the C2 position of the imidazole ring is easily protonated, resulting in poor cathodic stability^[31]. According to previous research, this problem was ameliorated by the introduction of phosphorus functional groups^[32]. The use of phosphonate-functionalized ILs (PFILs) is proposed in this work as an electrolyte co-solvent to suppress the oxidative dissolution of the Al current collector. The impact of the PFILs on the electrochemical properties of the high-voltage

Li||LiNi_{0.8}Co_{0.1}Mn_{0.1}O₂ (Li||NCM811) cell is investigated to reveal the working mechanism of the PFILs. The cathodic aluminum dissolution mechanism in the electrolytes with and without PFILs is shown in [Figure 1](#). After cycling, the TFSI⁻ anion attacks the Al₂O₃ passivation layer on fresh Al foils to form the corrosion product Al-TFSI compounds^[1,13,33] [[Figure 1B](#)]. On the contrary, after adding PFIL, a protective layer dominated by Li_xPO_yF_z is generated on the surface of Al foils, which can prevent Al corrosion caused by LiTFSI [[Figure 1C](#)].

EXPERIMENTAL

Materials

Bis (trifluoro methane sulfone) imide lithium salt (LiTFSI, 99.9%), ethylene carbonate (EC), and dimethyl carbonate (DMC), diethyl (3-bromopropyl) phosphonate (95%), 1-hexylimidazole (99%), ethyl acetate (EtOAc, 99%), dichloromethane (CH₂Cl₂, 99%), Silver nitrate (AgNO₃, 99%), and N-methyl-2-pyrrolidone (NMP, 99%) were purchased from Macklin. LiNi_{0.8}Mn_{0.1}Co_{0.1}O₂ (NCM811), poly (vinylidene fluoride) (PVDF), and conductive carbon black (Super P) were purchased from Guangdong Canrd New Energy Technology Co., Ltd.

Preparation of PFIL

The synthetic route of PFIL is shown in [Figure 2](#). Detailed synthetic steps are shown in the [Supplementary Material](#).

Structural characterization of PFIL

Fourier transform infrared spectroscopy (FT-IR) was recorded on a Nicolet 6700 FT-IR spectrometer (Thermo Fisher). ³¹P nuclear magnetic resonance (NMR), ¹H NMR, and ¹³C NMR of PFIL were recorded on a Bruker AV-400 NMR spectrometer in CDCl₃. NMR spectrogram analysis is shown in the [Supplementary Material](#). ³¹P NMR, ¹H NMR, and ¹³C NMR spectra of PFIL are presented in [Supplementary Figures 1-3](#), which confirms the synthesis of the PFIL molecule.

Purity characterization of PFIL

The water content of PFIL was measured by a Karl Fischer moisture meter (870 KF Titrino plus), and the result showed that the water content of PFIL was 0.26% [[Supplementary Table 1](#)]. To determine the halide content of PFIL, ion chromatography was conducted using a Thermo Fisher Aquion instrument with the pre-processing method of combustion in an oxygen bomb. The bromine content was found to be less than 50 ppm [[Supplementary Figure 4](#)], indicating that the bromide ions were almost completely exchanged during the synthesis process of PFIL.

Electrochemical measurements

The base electrolyte was prepared by dissolving 1.0 M LiTFSI in the solvent mixture of EC and DMC (1:1 by volume). In comparison, the hybrid electrolyte, which contained 20% PFIL and 80% base electrolyte, was prepared in the glove box (Mikrouna, China). To prepare the NCM811 electrode, NCM811 was employed as the active material, super P served as the electron conductive agent, and PVDF acted as the binder. These components were mixed in NMP with a weight ratio of 8:1:1. The slurry was coated onto an Al foil and further dried at 120 °C under vacuum for 24 h. The NCM811 electrode was punched into 12 mm diameter disks for testing and transferred into an Ar-filled glove box for cell assembly.

All electrochemical performances were conducted using the coin cells (CR2032) with lithium foils as the counter electrode, which were assembled in an Ar-filled glove box and operated with a CHI-660E workstation (Chenhua, Shanghai). Galvanostatic charge and discharge measurements were performed on a LAND battery system (Wuhan, China). The cut-off voltages were set to 3.0-4.4 V for the Li||NCM811 half-

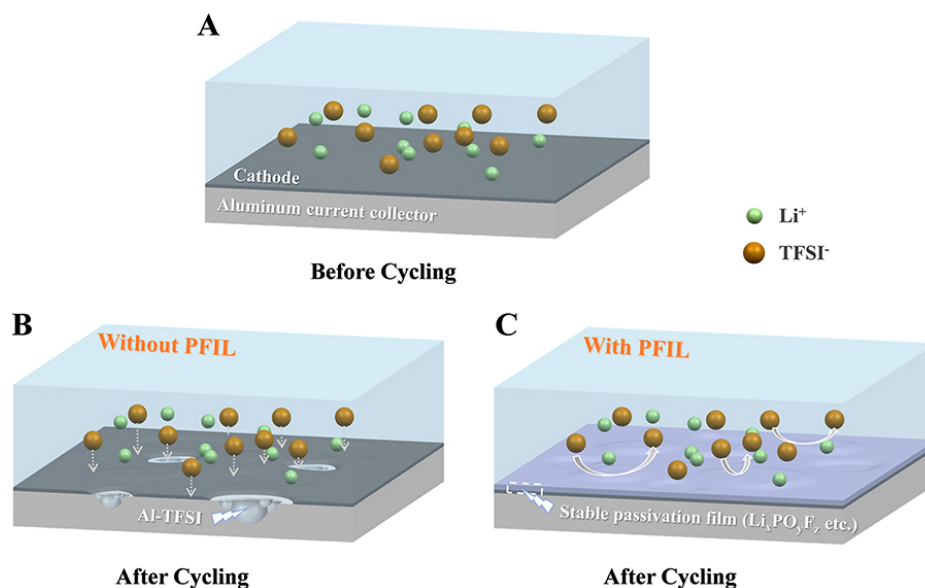


Figure 1. Schematic diagram before cycling (A) schematic illustration of the cathodic aluminum dissolution mechanism in the electrolyte without PFIL (B) and the electrolyte with PFIL (C) after cycling.

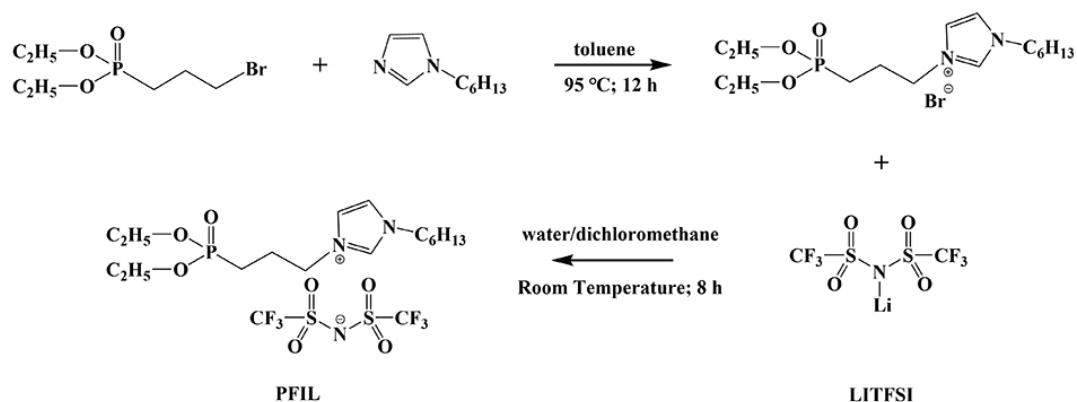


Figure 2. The synthetic route of PFIL.

cell. The AC impedance combined with the chrono-amperometry was applied to examine the lithium (Li)-ion transference number (t_{Li^+}). A lithium symmetrical battery was used here. The electrochemical window of the electrolyte was investigated through linear sweep voltammetry (LSV) at room temperature, using a scan rate of 5 mV s^{-1} within the potential range of 3.0 V to 5.0 V. Cyclic voltammetry (CV) measurements were carried out in the potential range of 2.0-5.0 V for $\text{Li}||\text{Al}$ half-cell. An AC amplitude of 5 mV was used during the performance of electrochemical impedance spectroscopy (EIS) within a frequency range spanning from 0.01 Hz to 100 KHz. Ionic conductivities measurements were maintained on an FE38-standard (Mettler Toledo, Switzerland). Raman spectra were carried out to indicate the influence of adding PFIL to a base electrolyte.

For the analysis of surface chemistry and morphology of the Al current collector, all cells were disassembled in the glove box. The Al current collector was washed with DMC to remove electrolyte residual and dried at room temperature. The morphology of the Al current collector was observed by scanning electron

microscopy (SEM, Hitachi, Japan). The surface chemistry of the Al current collector was examined by X-ray photoelectron spectroscopy (XPS, ESCALAB 250Xi).

RESULTS AND DISCUSSION

As we all know, the conductivity, viscosity, and flammability of the electrolyte are crucial for the performance of the LIBs. [Figure 3A](#) shows the viscosity and conductivity change before and after the addition of 20 wt% PFIL. When the temperature increases, the viscosity decreases, and the conductivity increases. Because the viscosity of the PFIL is higher than that of the organic carbonate solvent, the viscosity of the hybrid electrolyte is slightly higher than the base electrolyte, and the conductivity decreases at the same temperature. The conductivity meets the requirements of the LIBs. As shown in [Figure 3B](#), the self-extinguishing time (SET) is used to test the flammability of the electrolyte. With increasing PFIL content, the SET value gradually decreases, which is 174.1 s g^{-1} when 20 wt% of PFIL is added. With the addition of 80 wt% of PFIL, the electrolyte is completely non-flammable. The results confirm that the PFIL additive can significantly enhance the safety of the electrolyte.

The calculation of the t_{Li^+} was conducted using the Bruce-Vincent-Evans equation. The t_{Li^+} of the hybrid electrolyte is 0.46, which is much higher than that of the base electrolyte (0.35) in [Figure 4A](#) and [B](#). The increase of the t_{Li^+} is ascribed to the lone pair electrons of the PFIL cation, which has the ability to strongly coordinate Li-ions.

It is well known that the introduction of functional groups in ILs is done to demonstrate their impact on the physicochemical and electrochemical properties of electrolytes through the interaction between the functional groups and Li-ions^[34-36]. Raman spectroscopy is applied to detect the changes of ion-ion and ion-solvent interactions in the electrolytes^[37-39]. [Figure 5A](#) shows the Raman spectra of the interaction of PFIL with LiTFSI. The peak at 747 cm^{-1} corresponds to the bending vibration of the S-N-S group in LiTFSI, and its intensity significantly increases with the addition of PFIL to the base electrolyte. Moreover, the peak located at 900 cm^{-1} belongs to symmetrical stretching vibration of the O=S=O group, where the intensity is slightly enhanced with the addition of PFIL. Based on these results, it is clearly indicated that the solvation of Li-ions is caused by the coordination of the phosphonate group on cation, thereby weakening the interaction between Li-ions and bis (trifluoro methane sulfonyl) imide anions. This is the reason for the increased Li-ion transfer number.

The rate performance test is performed at the current density sequence of 0.5 C, 1 C, 2 C, 3 C, and 5 C, respectively [[Supplementary Figures 5-7](#)]. Better rate performance is exhibited when PFIL is used. At 0.5 C, the capacity exhibited by the base electrolyte is similar to that of the cell cycled with PFIL. However, the capacity difference is enlarged along with increasing current densities. The cell utilizing the PFIL electrolyte exhibits a capacity of 124 $mAh g^{-1}$, whereas the cell employing the base electrolyte only reaches around 108 $mAh g^{-1}$, particularly at 5 C. This improved rate performance can be attributed to the increased Li-ion migration in the electrolyte induced by PFIL.

The electrochemical stabilities of the electrolytes are investigated by LSV. [Figure 5B](#) shows the LSV curves of the electrolyte without PFIL and the electrolyte with PFIL. The electrochemical oxidation of the electrolyte with PFIL exhibits an onset voltage of 5.1 V, which is 0.2 V higher compared to the electrolyte without PFIL. As already reported, introducing functionalized group into the cations of the imidazole-based IL could increase the electrochemical stability, which sufficiently improves the electrochemical stability of electrolytes^[40]. The phosphonate functional group incorporated into the cation of the imidazole-based ILs enables PFIL to be a promising alternative electrolyte for LIBs.

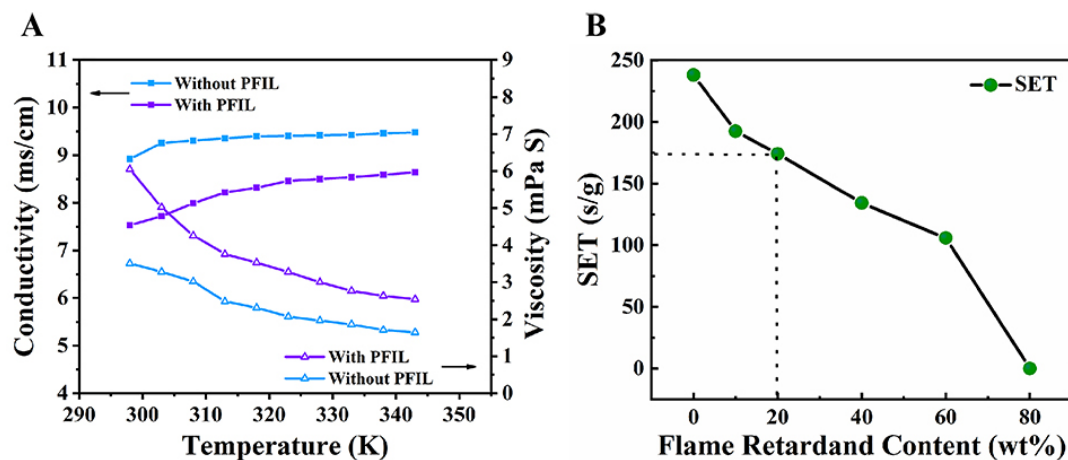


Figure 3. Temperature-dependent ionic conductivity of the electrolyte without PFIL and the electrolyte with 20 wt% of PFIL (A); Self-extinguishing time (SET) of the electrolytes with different PFIL contents (B).

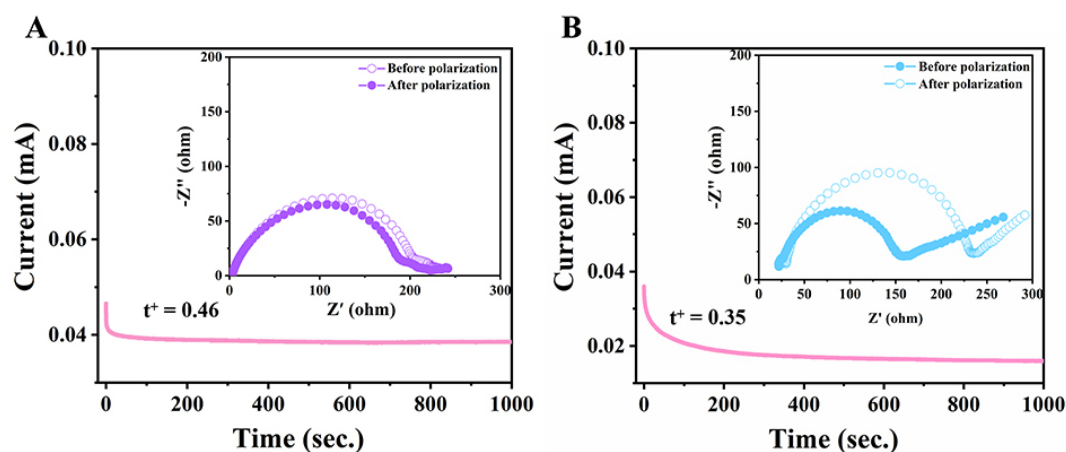


Figure 4. AC impedance spectra and chrono-amperometry curves of the electrolyte without PFIL (A) and the electrolyte with PFIL (B).

To investigate the corrosion of Al foils by LiTFSI, CV measurements are applied to the Li||Al cells cycled with the base and hybrid electrolytes, respectively [Figure 5C and D]. At the first scan, the corrosion current of the cells using the base electrolyte begins to rise after 4.2 V. When the amount of PFIL is 20 wt%; the corrosion current begins to rise after 4.6 V. The magnitude of the corrosion current density is significantly different at 5 V. The corrosion current density of the base electrolyte is 1.67 mA cm^{-2} , and the current drops to 0.186 mA cm^{-2} when PFIL is added to the base electrolyte. The Al foils in the base electrolyte exhibit a higher anodic current density, which indicates severe Al current collector corrosion. Those results can fully explain the inhibition of Al current collector corrosion by PFIL. Meanwhile, to properly evaluate the corrosion inhibition effect of the phosphonium-functionalized imidazolium IL (PFIL), we conducted CV tests on Li||Al batteries using electrolytes containing 20 wt% of non-functionalized imidazolium ILs [FIL; 1-hexyl-3-methylimidazolium bis(trifluoromethylsulfonyl)imide] and electrolytes containing 20 wt% of BMPyrr TFSI, respectively [Supplementary Figures 8 and 9]. An Al foil shows a lower corrosion current in the electrolyte containing 20 wt% PFIL, which indicates that PFIL has a better inhibition effect on the corrosion of the Al current collector.

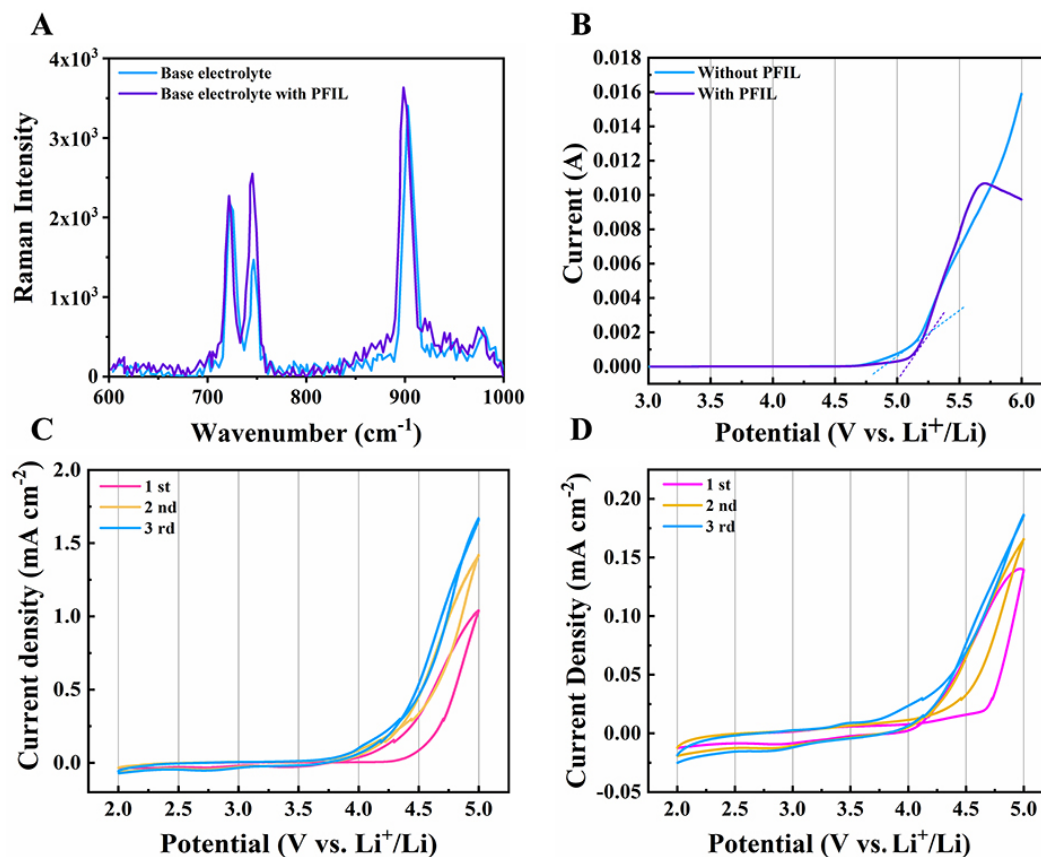


Figure 5. Raman spectra of the electrolyte without PFIL and the electrolyte with PFIL (A); LSV voltammograms of the electrolyte without PFIL and the electrolyte with PFIL (B); cyclic voltammetry of the Al electrodes in the electrolyte without PFIL (C) and the electrolyte with PFIL (D), respectively.

To further characterize the corrosion of the Al current collector induced by LiTFSI, the Al foils from the Li||Al cell was extracted after the CV measurement (2-5 V vs. Li/Li⁺). Subsequently, it was rinsed with DMC and subjected to SEM measurements [Figure 6]. The surface structures of the Al foils cycled with the electrolyte without PFIL and the electrolyte with PFIL are significantly different. No holes are found on the surface of the Al current collector before the CV test. However, there are many corrosion holes on the surface of the Al current collector cycled with the electrolyte without PFIL. Compared with the electrolyte without PFIL, the dissolution behavior of the Al current collector in the electrolyte with PFIL is suppressed, where no obvious corrosion holes are observed. PFIL induces the formation of a passivation layer on the surface of the Al current collector, which effectively prevents the dissolution of the Al collector and thus reduces the side reactions caused by LiTFSI. This is in line with the above CV measurement results.

XPS is applied to analyze the chemical composition at the surface of the Al foils [Figure 7]. For Al 2p spectra [Figure 7A], the peaks at 75.6 eV, 74.6 eV, and 71.9 eV correspond to Al-F, Al₂O₃, and Al, respectively^[1,33]. The peaks of Al₂O₃ and Al with the hybrid electrolyte are much stronger than the base electrolyte. The Al-F peak is only present on the Al foil after cycling in the basic electrolyte, while it is absent on the Al foil after cycling in the hybrid electrolyte, indicating that the presence of PFIL can suppress the corrosion of the Al current collector by LiTFSI. Moreover, in the O 1s spectra [Figure 7C], the peak assigned to Al₂O₃ (531.0 eV)^[29] with the base electrolyte is much weaker, which is consistent with the Al 2p spectra. The peaks belonging to C-F (687.7 eV) and LiF (685.5 eV) are both present in the F 1s spectra of the Al foils cycled

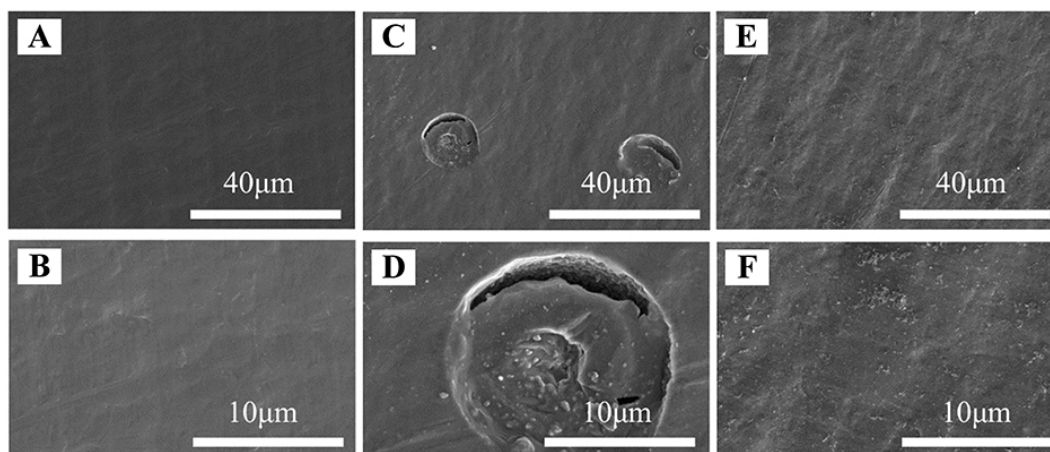


Figure 6. SEM morphologies of the fresh Al foils (A and B), the Al foils after a CV test in the electrolyte without PFIL (C and D), and the electrolyte with PFIL (E and F).

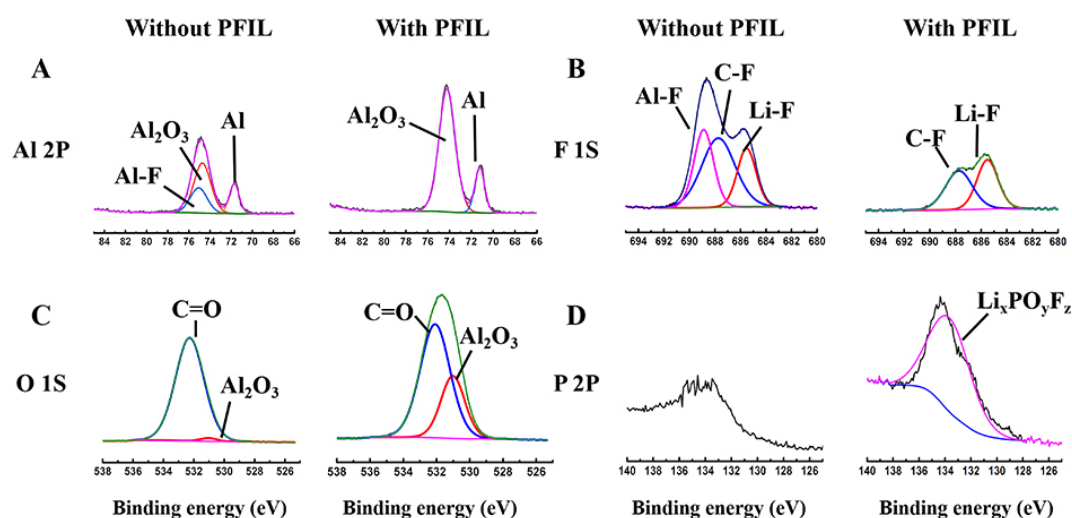


Figure 7. XPS spectra of the Al foils cycled in the electrolyte with PFIL and the electrolyte without PFIL.

with the base and hybrid electrolytes^[41-43]. In addition, the presence of Al-F (688.9 eV) on the Al surface cycled with the base electrolyte is good evidence indicating the corrosion of the Al current collector by LiTFSI. This result suggests that the Al foils exposed to the base electrolyte are corroded severely. In the F 1s spectra [Figure 7B], the LiF peak of the Al foils exposed to the base electrolyte is higher than that of the hybrid electrolyte, indicating existence of more LiF with the base electrolyte. LiF has a negative effect on the interface impedance, which reduces the electrochemical performance of the battery. The peak of 133.9 eV in the P 2p spectrum [Figure 7D] corresponds to $\text{Li}_x\text{PO}_y\text{F}_z$, which is caused by the decomposition of phosphorus functional groups in the hybrid electrolyte^[32,44]. The base electrolyte (LiTFSI + EC/DMC) does not contain the P element, confirming that the P element exists only in PFIL, which proves that PFIL participates in the interface reaction and forms a passivation layer on the surface of the Al foils.

According to the above analysis, it is speculated that the TFSI⁻ anion attacks the Al_2O_3 passivation layer on fresh Al foils to form the corrosion product Al-TFSI compounds. The compounds can be dissolved by the carbonate solvent. With the failure of the Al_2O_3 passivation layer, Al is exposed to the electrolyte and begins

to be dissolved continuously at high potential. On the contrary, after adding PFIL, a protective layer dominated by $\text{Li}_x\text{PO}_y\text{F}_z$ is generated on the surface of Al foils, which can prevent Al corrosion caused by LiTFSI according to the SEM results.

The cycling performance of the Li||NCM811 cell is evaluated with four initial cycles at 0.1 C, followed by further cycles at 0.5 C [Figure 8A]. The cell utilizing the base electrolyte exhibits a discharge capacity of 196.1 mAh g⁻¹ and an initial coulombic efficiency of 89.3%. In contrast, the battery with the hybrid electrolyte shows a discharge capacity of 204.7 mAh g⁻¹ with the coulombic efficiency of 86.0%. The decreased coulombic efficiency by the PFIL-containing electrolyte implies that PFIL is involved in CEI formation. When cycled at 0.5 C, the initial capacity of the base electrolyte is comparable to that of the hybrid electrolyte. However, the capacity drops to 108.2 mAh g⁻¹ after 50 cycles, which is lower than that of the hybrid electrolyte (121.3 mAh g⁻¹). Correspondingly, the capacity retention of the base electrolyte is much lower compared to the hybrid electrolyte (66.7% vs. 73.0%). After 80 cycles, the coulombic efficiency and capacity of the cell using the base electrolyte drop sharply, while the cell using the hybrid electrolyte maintains a high coulombic efficiency and high capacity. After 100 cycles, the battery employing the base electrolyte demonstrates a significantly reduced capacity of only 32.9 mAh g⁻¹, accompanied by a coulombic efficiency of 81.8%. In contrast, the cell utilizing the hybrid electrolyte maintains a higher capacity of 99.5 mAh g⁻¹ and exhibits an impressive coulombic efficiency of 99.2%. The improved cycling performance of the hybrid electrolyte originates from the corrosion suppression of the Al current collector assisted by the PFIL additive. Meanwhile, the performance of NMC811 cathode material for LIBs with different electrolytes was obtained from the literature, as shown in Table 1.

EIS is conducted to further explore the influence of PFIL on the electrochemical performance of the Li||NCM811 cell. Supplementary Figure 10 shows the corresponding equivalent circuit model, which indicates the bulk electrolyte resistance (R_1), the parallel combination of SEI resistance (R_{sei}), and charges transfer resistance (R_{ct}) with a constant phase element (CPE). The Warburg impedance is represented by the straight line observed in the low-frequency region^[48]. As shown in Figure 8B and C, the battery using the electrolyte with PFIL has smaller R_{sei} and R_{ct} than the electrolyte without PFIL. It indicates that the impedance of the interfacial layer formed in the electrolyte with PFIL is lower than that of the electrolyte without PFIL, resulting in improved cycling performance. Meanwhile, the additional semicircle observed in the low-frequency region may be related to the corrosion of Al that occurs in the electrolyte without PFIL^[49].

The impedance data of the battery after different cycles in the electrolyte without PFIL and the electrolyte with PFIL are shown in Table 2. After the first cycle, the R_{sei} and R_{ct} of the electrolyte with PFIL are slightly higher than that of the electrolyte without PFIL, which may be caused by the formation of a stable interfacial film in the electrolyte with PFIL. As the cycle proceeds, the R_{ct} of the electrolyte without PFIL cells is significantly larger by an order of magnitude after the 10th cycle than the R_{ct} of the electrolyte with PFIL cells. The significant difference is attributed to aluminum corrosion. On the one hand, the corrosion of the collector will make the active material lose electrical contact with the external circuit, which significantly increases the difficulty of electron transfer. On the other hand, the corrosion of Al by LiTFSI causes continuous decomposition of electrolytes and thickens the positive electrode surface film, which leads to the deterioration of positive electrode charge diffusion kinetics.

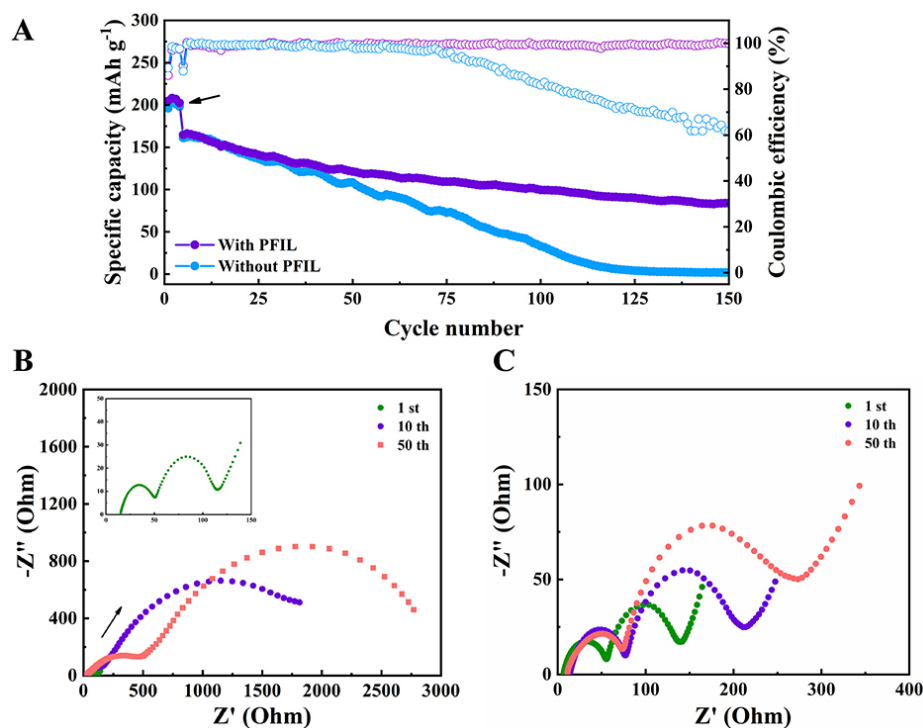
In order to observe the corrosion of the Al current collector caused by LiTFSI, the morphology of the Al current collector of cycled Li||NCM811 cell is characterized by SEM. Before cycling, it is evident that the fresh Al foils [Figure 9A] exhibit a smooth surface. However, after cycling with the base electrolyte, the Al current collector [Figure 9B] shows numerous corrosion holes. The existence of the corrosion holes not

Table 1. Performance data of Li|NCM811 batteries with different electrolytes

Electrolyte	Test condition	Initial discharge specific capacity	Initial coulombic efficiency	After 100 cycles	References
1M LiTFSI + EC/DMC (1:1)	1 C = 200 mA/g; 3.0-4.4 V; 0.5 C; 25 °C	196.1 mAh/g	89.3%	16.8%	/
0.2M PFIL + 0.8M LiTFSI + EC/DMC (1:1)	1 C = 200 mA/g; 3.0-4.4 V; 0.5 C; 25 °C	204.7 mAh/g	86.0%	48.6%	/
1M LiPF ₆ + EC/DMC/EMC (1:1:1)	1 C = 200 mA/g; 2.5-4.5 V; 0.2 C; 25 °C	198.2 mAh/g	86.1%	51.0%	[45]
1M LiPF ₆ + EC/DMC (1:2)	1 C = 200 mA/g; 3.0-4.3 V; 0.5 C; 60 °C	220.8 mAh/g	88.1%	46.4%	[46]
1M LiPF ₆ + EC/DEC/EMC (1:1:1)	1 C = 200 mA/g; 2.7-4.3 V; 1 C; 25 °C	152.9 mAh/g	/	78.37%	[47]

Table 2. Fitted data for the EIS spectra of NCM811 cells with and without PFIL

Sample	After one cycle			After ten cycles		After 50 cycles	
R (Ω)	R _{sei} (Ω)	R _{ct} (Ω)	R _{sei} (Ω)	R _{ct} (Ω)	R _{sei} (Ω)	R _{ct} (Ω)	
With PFIL	51.04	90.29	68.10	141.20	75.8	219.1	
Without PFIL	39.86	72.33	99.56	2,236	318.8	2,946	

**Figure 8.** Cycling performance and coulombic efficiency of Li|NCM811 cells with the electrolyte without PFIL and the electrolyte with PFIL (A) with the first four cycles at 0.1 C and following cycles at 0.5 C; Nyquist plots of Li|NCM811 cells cycled in the electrolyte without PFIL (B) and the electrolyte with PFIL (C), respectively.

only aggravates the polarization of the battery but also leads to rapid attenuation of the battery capacity. In contrast, the Al foils of the cell cycled with the hybrid electrolyte are smooth and flat [Figure 9C]. The inclusion of PFIL is further evidence of its ability to inhibit surface corrosion of the Al current collector caused by LiTFSI over multiple cycles.

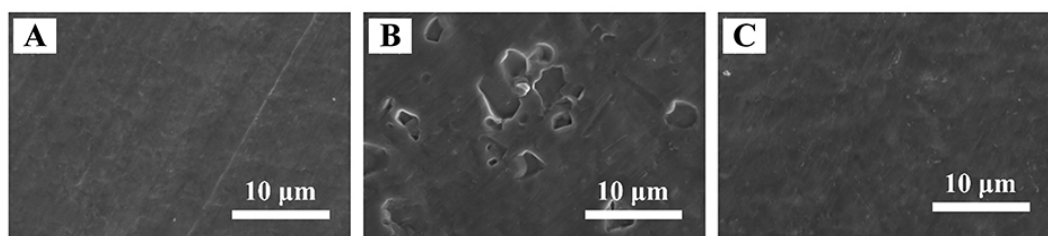


Figure 9. SEM morphologies of the fresh Al foils (A) and the Al foils cycled in the electrolyte without PFIL (B) and the electrolyte with PFIL (C).

CONCLUSIONS

In summary, PFIL is synthesized and utilized as an electrolyte co-solvent in the Li||NCM811 cell. The oxidation dissolution of the Al collector induced by LiTFSI is effectively suppressed by PFIL, resulting in significantly improved cycling and rate performances. The addition of PFIL considerably reduces the corrosion current density from 1.67 mA cm^{-2} to 0.186 mA cm^{-2} according to the result of CV, which proves that PFIL inhibits the Al current collector corrosion. The XPS confirms that PFIL is involved in the interface reaction, forming a stable passivation film rich in $\text{Li}_x\text{PO}_y\text{F}_z$ on the surface of the Al foil, which can effectively improve Li-ion transportation. The Li||NCM811 cell with the hybrid electrolyte shows a more stable cycling performance than the cell cycled with the base electrolyte. After 100 cycles at 0.5 C, a capacity of 99.5 mAh g^{-1} can be maintained, with a high coulombic efficiency of 99.2%. In contrast, the battery cycled with the base electrolyte only exhibits a capacity of 32.9 mAh g^{-1} and a coulombic efficiency of 81.8%. In general, the Li||NCM811 cell with the hybrid electrolyte shows better cycling performance and improved capacity retention due to corrosion inhibition of the Al current collector. This work provides an effective strategy for the development of stable high-voltage LIBs.

DECLARATIONS

Authors' contributions

Carried out laboratory research and manuscript writing: Liao K, Song J

Carried out materials testing and characterization: Ge J

Carried out material synthesis: Si J

Contributed to the literature research: Cai Y, Luo Z

Carried out student supervision, concept development, funding acquisition, and manuscript revision: Zhou M, Liang H, Cheng YJ, Milanovic M, Inoishi A, Okada S

Availability of data and materials

Available upon request from the authors.

Financial support and sponsorship

This work was financially supported by the Municipal Key R&D Program of Ningbo (2020Z024, 2021Z121, 2022Z096, 2022Z158, 2022Z115, 2023Z064) and sponsored by K.C. Wong Magna Fund at Ningbo University.

Conflicts of interest

All authors declared that there are no conflicts of interest.

Ethical approval and consent to participate

Not applicable.

Consent for publication

Not applicable.

Copyright

© The Author(s) 2023.

REFERENCES

1. Shangguan X, Jia G, Li F, et al. 1-ethyl-3-methyl-imidazolium bis (trifluoromethane-sulfonyl) imide as an electrolyte additive in LiFePO₄-based batteries for suppressing aluminum corrosion. *Energy Technol* 2018;6:1667-74. DOI
2. Liu Z, Chai J, Xu G, Wang Q, Cui G. Functional lithium borate salts and their potential application in high performance lithium batteries. *Coord Chem Rev* 2015;292:56-73. DOI
3. Li J, Xie K, Lai Y, et al. Lithium oxalyldifluoroborate/carbonate electrolytes for LiFePO₄/artificial graphite lithium-ion cells. *J Power Sources* 2010;195:5344-50. DOI
4. Kaymaksiz S, Wilhelm F, Wachtler M, et al. Electrochemical stability of lithium salicylato-borates as electrolyte additives in Li-ion batteries. *J Power Sources* 2013;239:659-69. DOI
5. Li S, Zhao W, Zhou Z, et al. Studies on electrochemical performances of novel electrolytes for wide-temperature-range lithium-ion batteries. *ACS Appl Mater Inter* 2014;6:4920-6. DOI
6. Andersson AM, Edström K. Chemical composition and morphology of the elevated temperature SEI on graphite. *J Electrochem Soc* 2001;148:A1100. DOI
7. Sloop SE, Pugh JK, Wang S, Kerr JB, Kinoshita K. Chemical reactivity of PF₅ and LiPF₆ in ethylene carbonate/dimethyl carbonate solutions. *ECS Solid State Lett* 2001;4:A42. DOI
8. Kanamura K, Takezawa H, Shiraishi S, Takehara Z. Chemical reaction of lithium surface during immersion in LiClO₄ or LiPF₆/DEC electrolyte. *J Electrochem Soc* 1997;144:1900-6. DOI
9. Zhou G, Sun X, Li QH, et al. Mn Ion dissolution mechanism for lithium-ion battery with LiMn₂O₄ cathode: *in situ* ultraviolet-visible spectroscopy and Ab initio molecular dynamics simulations. *J Phys Chem Lett* 2020;11:3051-7. DOI
10. Lin C, Tang A, Mu H, Wang W, Wang C. Aging mechanisms of electrode materials in lithium-ion batteries for electric vehicles. *J Chem* 2015;2015:104673. DOI
11. Tebbe JL, Fuerst TF, Musgrave CB. Mechanism of hydrofluoric acid formation in ethylene carbonate electrolytes with fluorine salt additives. *J Power Sources* 2015;297:427-35. DOI
12. Dahbi M, Ghamouss F, Tran-van F, Lemordant D, Anouti M. Comparative study of EC/DMC LiTFSI and LiPF₆ electrolytes for electrochemical storage. *J Power Sources* 2011;196:9743-50. DOI
13. Gabryelczyk A, Ivanov S, Bund A, Lota G. Corrosion of aluminium current collector in lithium-ion batteries: a review. *J Energy Storage* 2021;43:103226. DOI
14. Bushkova OV, Yaroslavtseva TV, Dobrovolsky YA. New lithium salts in electrolytes for lithium-ion batteries (Review). *Russ J Electrochem* 2017;53:677-99. DOI
15. Bizot C, Blin M, Guichard P, et al. Aluminum current collector for high voltage Li-ion battery. Part I: a benchmark study with statistical analysis. *Electrochem Commun* 2021;126:107013. DOI
16. Naoi K, Mori M, Naruoka Y, Lamanna WM, Atanasoski R. The surface film formed on a lithium metal electrode in a new imide electrolyte, lithium bis(perfluoroethylsulfonylimide) [LiN(C₂F₅SO₂)₂]. *J Electrochem Soc* 1999;146:462. DOI
17. Han H, Zhou S, Zhang D, et al. Lithium bis(fluorosulfonyl)imide (LiFSI) as conducting salt for nonaqueous liquid electrolytes for lithium-ion batteries: physicochemical and electrochemical properties. *J Power Sources* 2011;196:3623-32. DOI
18. Meister P, Qi X, Kloepsch R, et al. Anodic behavior of the aluminum current collector in imide-based electrolytes: influence of solvent, operating temperature, and native oxide-layer thickness. *ChemSusChem* 2017;10:804-14. DOI
19. Yen C, Neale AR, Lim J, Bresser D, Hardwick LJ, Hu C. Corrosion suppression of aluminium current collectors within Li-ion cells using 3-methoxypropionitrile-based electrolytes. *Electrochim Acta* 2022;431:141105. DOI
20. Abouimrane A, Ding J, Davidson I. Liquid electrolyte based on lithium bis-fluorosulfonyl imide salt: aluminum corrosion studies and lithium ion battery investigations. *J Power Sources* 2009;189:693-6. DOI
21. Dahbi M, Ghamouss F, Tran-van F, Lemordant D, Anouti M. Ester based electrolyte with lithium bis(trifluoromethane sulfonyl) imide salt for electrochemical storage devices: physicochemical and electrochemical characterization. *Electrochim Acta* 2012;86:287-93. DOI
22. Chen X, Xu W, Engelhard MH, et al. Mixed salts of LiTFSI and LiBOB for stable LiFePO₄-based batteries at elevated temperatures. *J Mater Chem A* 2014;2:2346-52. DOI
23. Li F, Gong Y, Jia G, et al. A novel dual-salts of LiTFSI and LiODFB in LiFePO₄-based batteries for suppressing aluminum corrosion and improving cycling stability. *J Power Sources* 2015;295:47-54. DOI

24. Pan Y, Wang G, Lucht BL. Cycling performance and surface analysis of lithium bis(trifluoromethanesulfonyl)imide in propylene carbonate with graphite. *Electrochim Acta* 2016;217:269-73. DOI
25. Krämer E, Schedlbauer T, Hoffmann B, et al. Mechanism of anodic dissolution of the aluminum current collector in 1 M LiTFSI EC:DEC 3:7 in rechargeable lithium batteries. *J Electrochem Soc* 2013;160:A356. DOI
26. Matsumoto K, Inoue K, Nakahara K, Yuge R, Noguchi T, Utsugi K. Suppression of aluminum corrosion by using high concentration LiTFSI electrolyte. *J Power Sources* 2013;231:234-8. DOI
27. Li R, Fang Z, Wang C, et al. Six-armed and dicationic polymeric ionic liquid for highly stretchable, nonflammable and notch-insensitive intrinsic self-healing solid-state polymer electrolyte for flexible and safe lithium batteries. *Chem Eng J* 2022;430:132706. DOI
28. Wang B, Wang G, He P, Fan L. Rational design of ultrathin composite solid-state electrolyte for high-performance lithium metal batteries. *J Membr Sci* 2022;642:119952. DOI
29. Peng C, Yang L, Zhang Z, Tachibana K, Yang Y, Zhao S. Investigation of the anodic behavior of Al current collector in room temperature ionic liquid electrolytes. *Electrochim Acta* 2008;53:4764-72. DOI
30. Liu K, Wang Z, Shi L, Jungstuiwong S, Yuan S. Ionic liquids for high performance lithium metal batteries. *J Energy Chem* 2021;59:320-33. DOI
31. Tang X, Lv S, Jiang K, Zhou G, Liu X. Recent development of ionic liquid-based electrolytes in lithium-ion batteries. *J Power Sources* 2022;542:231792. DOI
32. Ge J, Liang H, Zhou M, et al. Phosphonate-functionalized ionic liquid: a novel electrolyte additive for enhanced cyclic stability and rate capability of LiCoO₂ cathode at high voltage. *ChemistrySelect* 2019;4:9959-65. DOI
33. Morita M, Shibata T, Yoshimoto N, Ishikawa M. Anodic behavior of aluminum in organic solutions with different electrolytic salts for lithium ion batteries. *Electrochim Acta* 2002;47:2787-93. DOI
34. Mai YJ, Luo H, Zhao XY, et al. Organosilicon functionalized quaternary ammonium ionic liquids as electrolytes for lithium-ion batteries. *Ionics* 2014;20:1207-15. DOI
35. Fei Z, Geldbach TJ, Zhao D, Dyson PJ. From dysfunction to bis-function: on the design and applications of functionalised ionic liquids. *Chemistry* 2006;12:2122-30. DOI
36. Davis, Jr. J. Task-specific ionic liquids. *Chem Lett* 2004;33:1072-7. DOI
37. Seo DM, Borodin O, Han S, Boyle PD, Henderson WA. Electrolyte solvation and ionic association II. acetonitrile-lithium salt mixtures: highly dissociated salts. *J Electrochem Soc* 2012;159:A1489. DOI
38. Seo DM, Borodin O, Han S, Ly Q, Boyle PD, Henderson WA. Electrolyte solvation and ionic association. *J Electrochem Soc* 2012;159:A553. DOI
39. Umebayashi Y, Mitsugi T, Fukuda S, et al. Lithium ion solvation in room-temperature ionic liquids involving bis(trifluoromethanesulfonyl) imide anion studied by raman spectroscopy and DFT calculations. *J Phys Chem B* 2007;111:13028-32. DOI
40. Kakibe T, Ohata T, Saito T, et al. Branched alkyl functionalization of imidazolium-based ionic liquids for lithium secondary batteries. *Electrochemistry* 2022;90:037006. DOI
41. Li F, Liu J, He J, et al. Additive-assisted hydrophobic Li⁺-solvated structure for stabilizing dual electrode electrolyte interphases through suppressing LiPF₆ hydrolysis. *Angew Chem Int Ed* 2022;61:e202205091. DOI
42. Huang J, Liu J, He J, et al. Optimizing electrode/electrolyte interphases and Li-ion flux/solvation for lithium-metal batteries with quadrifunctional heptafluorobutyric anhydride. *Angew Chem Int Ed* 2021;60:20717-22. DOI
43. Qiao L, Oteo U, Martinez-Ibañez M, et al. Stable non-corrosive sulfonimide salt for 4-V-class lithium metal batteries. *Nat Mater* 2022;21:455-62. DOI
44. Zeng Z, Liu X, Jiang X, et al. Enabling an intrinsically safe and high-energy-density 4.5 V-class Li-ion battery with nonflammable electrolyte. *InfoMat* 2020;2:984-92. DOI
45. Wang Y, Dong N, Liu B, Tian G, Qi S, Wu D. Self-adaptive gel poly(imide-siloxane) binder ensuring stable cathode-electrolyte interface for achieving high-performance NCM811 cathode in lithium-ion batteries. *Energy Stor Mater* 2023;56:621-30. DOI
46. Kim JH, Kim H, Kim W, et al. Incorporation of titanium into Ni-rich layered cathode materials for lithium-ion batteries. *ACS Appl Energy Mater* 2020;3:12204-11. DOI
47. Wang L, Su Q, Shi W, et al. Optimized structure stability and cycling performance of LiNi_{0.8}Co_{0.1}Mn_{0.1}O₂ through homogeneous nano-thickness Al₂O₃ coating. *Electrochim Acta* 2022;435:141411. DOI
48. Liu Q, Yang G, Liu S, Han M, Wang Z, Chen L. Trimethyl borate as film-forming electrolyte additive to improve high-voltage performances. *ACS Appl Mater Interface* 2019;11:17435-43. DOI
49. Xue W, Wang Q, Sun G, Li Q, Yu X, Li H. Introducing competitive adsorption species in sulfonimide salt-based electrolytes for inhibiting aluminium corrosion. *Chem Commun* 2022;58:10341-4. DOI